Environmental Science and Pollution Research
https://doi.org/10.1007/s11356-018-3638-y

RESEARCH ARTICLE

Kinetic and equilibrium adsorption of two post-harvest fungicides onto copper-exchanged montmorillonite: synergic and antagonistic effects of both fungicides' presence

Martina Gamba[1] · Juan M. Lázaro-Martínez[2] · Melisa S. Olivelli[3] · Florencia Yarza[1] · Daniel Vega[4] · Gustavo Curutchet[3] · Rosa M. Torres Sánchez[1]

Received: 16 July 2018 / Accepted: 30 October 2018

Abstract

The simultaneous adsorption of both imazalil (IMZ) and thiabendazole (TBZ) fungicides in a Cu^{2+}-exchanged Mt was studied in this work. Kinetic studies were used to determine the rate law which describes the adsorption of individual fungicides onto the adsorbent. Adsorption isotherm of individual and combined fungicides was done to evaluate synergic or antagonistic effects. The Mt-Cu material considerably improved TBZ and/or IMZ adsorption from aqueous suspensions with respect to raw Mt, leading to removal efficiencies higher than 99% after 10 min of contact time for TBZ and IMZ C_i = 15 and 40 mg/L, respectively, when a solid dosage = 1 g/L was used. The adsorption sites involved were determined by a combination of X-ray diffraction (XRD) determinations and electron paramagnetic resonance (EPR), indicating that fungicides were bonded to Cu^{2+} cations, while the rate limiting step was the formation of coordination bonds. The adsorption mechanism proposed is that of ligand exchange between water and fungicide molecules in the metal coordination sphere. The single-crystal structure for the IMZ-Cu^{2+} complex indicated that four molecules were bounded to the copper centers, while two molecules of TBZ are bounded to copper explaining the higher IMZ uptake capacity for the Mt-Cu material.

Keywords Cu^{2+}-exchanged montmorillonite · Thiabendazole · Imazalil · Adsorption · Crystal structure determination · Copper-imazalil complex

Responsible editor: Tito Roberto Cadaval Jr

Electronic supplementary material The online version of this article (https://doi.org/10.1007/s11356-018-3638-y) contains supplementary material, which is available to authorized users.

✉ Rosa M. Torres Sánchez
rosats@cetmic.unlp.edu.ar

[1] CETMIC-CONICET-CCT La Plata-CIC, Camino Centenario y 506, (1897) M. B. Gonnet, La Plata, Argentina

[2] IQUIMEFA -CONICET, Facultad de Farmacia y Bioquímica, Departamento de Química Orgánica, Universidad de Buenos Aires, Junín 956 (1113), Buenos Aires, Argentina

[3] Escuela de Ciencia y Tecnología e Instituto de Investigación e Ingeniería Ambiental, CONICET, Universidad Nacional de San Martín, Av. 25 de Mayo y Francia, 1650 General San Martín, Buenos Aires, Argentina

[4] Departamento de Física de la Materia Condensada, Comisión Nacional de Energía Atómica, Av. Gral. Paz 1499 (1650) San Martín, Buenos Aires, Argentina

Introduction

Imazalil (IMZ) and thiabendazole (TBZ) are post-harvest fungicides, widely used in citrus and seed fruit packaging plants. They are applied in several steps during fruit processing, and consequently, high volumes of wastewater containing mixtures of fungicides and other chemical products are generated (Jiménez et al. 2015). IMZ is considered "likely to be carcinogen in humans" by USA Environmental Protection Agency (Environmental Protection Agency (EPA) n.d.-a), while TBZ shows generally low acute toxicity in humans but high toxicity to freshwater estuarine fish and freshwater/estuarine invertebrates (Environmental Protection Agency (EPA) n.d.-b). Thiabendazole has been detected in surface waters and sediment compartments (de Oliveira Neto OF et al. 2017).

The toxicity, bioaccumulation, and persistence in the environment of both fungicides generate concern regarding their effects on aquatic organisms. Furthermore, regulations regarding their maximum residue levels in commodities have

Published online: 23 November 2018

become more and more stringent since the amount of residual pesticides detected is increasing worldwide (Jiménez et al. 2015). Taking into account the presence of both fungicides in real agro-food wastewater (Jiménez-Tototzintle et al. 2015), it is necessary to develop methodologies for the simultaneous removal of both compounds prior to their discharge into natural waters.

Adsorption is a widely reported method to remove pesticides from wastewater, which does not lose validity due to its important advantages of being non-destructive, effective, inexpensive, and easy to apply.

Montmorillonite (Mt) is a smectite clay which behaves as a good adsorbent towards cationic species (Rytwo et al. 1995; Gürses et al. 2004; Parolo et al. 2008; Mazloomi and Jalali 2017). It presents a high specific surface area due to its colloidal size, permanent negative surface charge due to structural isomorphic substitutions, and a high cation exchange capacity, which allows the exchange of interlayer—natural occurring—inorganic cations with dissolved cationic species.

In previous studies, TBZ or IMZ adsorption onto montmorillonites (Mt) has been reported. Its uptake by raw Mt occurred through cation exchange reaction between the cationic form of the fungicides and inorganic interlayer cations, due to the basic character of the formers (Gamba et al. 2015, 2017a, 2017b; Lombardi et al. 2003, 2006; Roca Jalil et al. 2014). However, a way to improve the effectiveness of TBZ removal from water by the clay was found to be the exchange of Mt by Cu^{2+}, which acted as specific and high affinity TBZ adsorption site in the clay, since the neutral form of the fungicide coordinated with the metal center through imidazolic and thiazolic nitrogen atoms (Gamba et al. 2017b). It is expected that IMZ would behave in a similar manner than TBZ, taking into account the presence of both oxygen and nitrogen atoms with free electronic pairs in its structure. Furthermore, the complex formation between Cu^{2+} and two imidazole derivatives in Mt was reported by Holešová et al. (2009) and reinforces this hypothesis.

There is a lack of information about the TBZ and IMZ simultaneous or consecutive adsorption onto a single adsorbent. For this reason, the objective of this study was to evaluate the adsorption of both fungicides on a Cu^{2+}-exchanged Mt and to assess synergic or antagonistic effects during the simultaneous fungicide adsorption. Particularly, kinetic studies carried on individual fungicide adsorption allowed determining the rate law which describes the adsorption phenomenon. The adsorption sites and mechanism involved were evidenced by X-ray diffraction (XRD) and electron paramagnetic resonance (EPR) of materials. The single-crystal structure for the IMZ-Cu^{2+} complex was solved with the aim of establishing the number of imazalil molecules bounded to each Cu^{2+} cation.

The outlined strategy would enable to develop a two-step remediation process where the same raw material (Mt) is used for the removal of transition metals from industrial and/or mining effluents and the exchanged Mt product is used in further remediation processes to remove pesticides from agricultural effluents.

Materials and methods

Materials

A Patagonian (Rio Negro Province, Argentina) Mt sample, provided by Castiglioni Pes y Cia., was previously characterized (Gamba et al. 2015; Magnoli et al. 2008) and used as received.

The Cu^{2+}-exchanged Mt (labeled as Mt-Cu) was obtained following the methodology described in Gamba et al. (2017b). Briefly, 10 g of sample was dispersed in 500 mL of water, and a Cu^{2+} ($CuSO_4.5H_2O$) amount equivalent to 1.5 CEC (0.825 mmol/g clay, Gamba et al. 2015) was slowly added. The suspension was stirred overnight at 25 °C. The pH value of the suspension was 4.8. The product was rinsed three times with deionized water, dried at 80 °C, and ground in an agate mortar.

The fungicide TBZ (Fig. 1a), IUPAC chemical formula 2-(thiazol-4-yl) benzimidazole, was supplied by Fluka (Buchs, Switzerland) (98% purity) and used as received. It is a solid crystalline substance with molar mass (MM) = 201.3 g/mol, solubility in water of 160 mg/L at pH 4 and 30 mg/L at pH 7–10, both at 20.0 ± 0.5 °C (Tway and Love 1982) and pK_as at 2.5; 4.7 and 12 (Roberts-Hutson 1998). The IUPAC name of IMZ (Fig. 1b) is (RS)-1-(β-allyloxy-2,4-dichlorophenylethyl) imidazole; its solubility in water is 0.184 g/L at 20.0 ± 0.5 °C; its MM = 297.2 g/mol and pKa = 6.49. It was supplied by Sigma-Aldrich (p.a.) and used as received. The more restrictive regulation for drinking water establishes the maximum admissible concentration for individual pesticides at 0.1 mg/L (Barahona et al. 2010).

IMZ-Cu^{2+} complex single-crystal suitable for X-ray analysis was obtained from a methanolic solution containing IMZ and Cu $(NO_3)_2$ in a relation 2:1 by slow evaporation of the solvent at room temperature.

Adsorption kinetics and adsorption isotherms

Fungicide adsorption kinetics and isotherms were carried out using the batch method. A weighed amount of TBZ or IMZ was dissolved in deionized water in order to prepare a 25- or 150-mg/L solution, respectively. Further concentrations were achieved by dilution in deionized water. Duplicates of Mt or Mt-Cu samples were weighed into 30-mL centrifuge tubes, and the corresponding fungicide solution was added. The suspensions were stirred (150 rpm) during a certain contact time at 25 °C. Clay/solution ratios, fungicide concentrations,

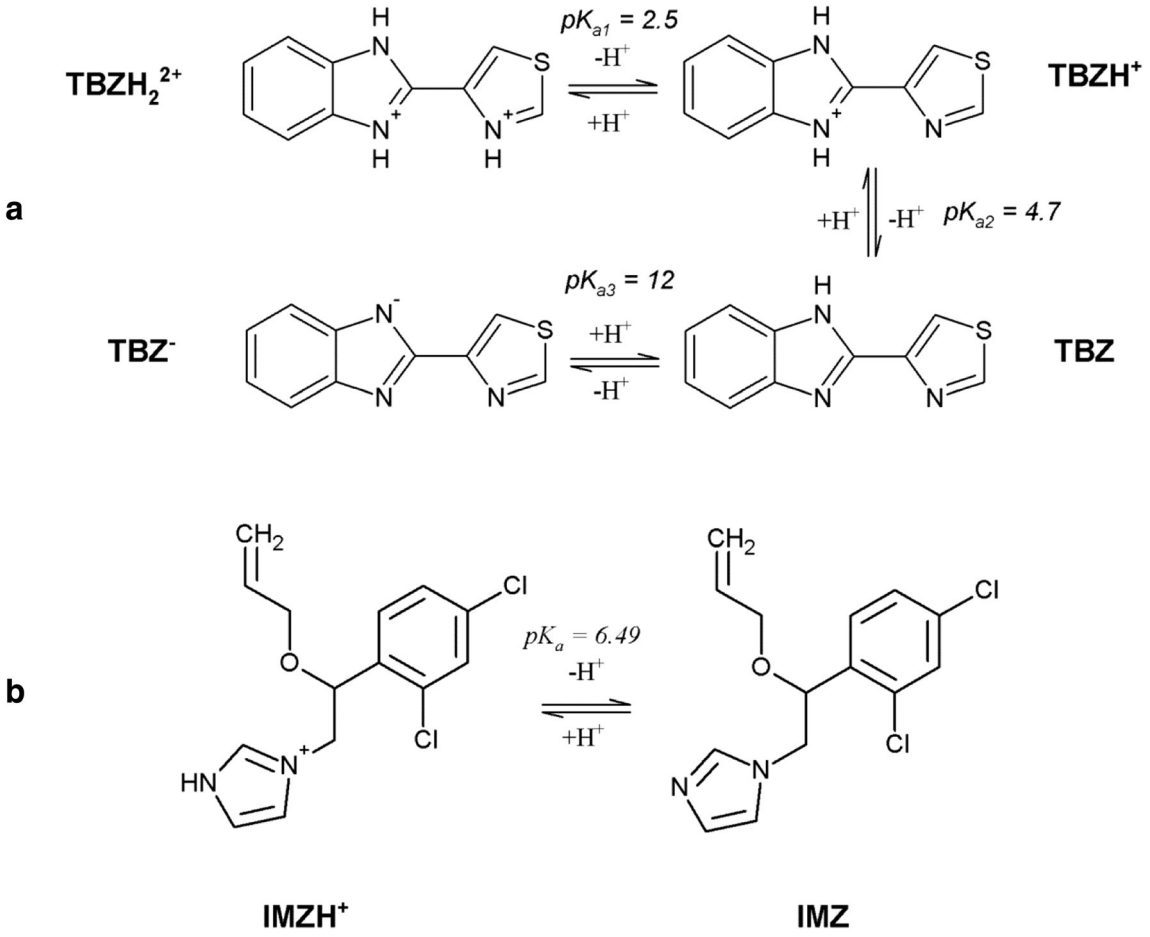

Fig. 1 Chemical structures of (**a**) thiabendazole and (**b**) imazalil

contact time used in adsorption experiments (kinetics and equilibrium studies), and labeled products were shown in Table 1.

After contact time, the suspensions were centrifuged at 14,000 rpm for 15 min to separate the solid products. The concentrations of TBZ and/or IMZ in the supernatants were analyzed by high-performance liquid chromatography (HPLC) coupled with UV–visible ($\lambda = 298$ for TBZ and $\lambda = 220$ nm for IMZ) and fluorescence ($\lambda_{ex} = 300$ nm and $\lambda_{em} = 350$ nm for TBZ) detection using a Shimadzu HPLC C18 column (4.6 mm × 250 mm, 4.6 μm). The injected volume was 10 μL and the mobile phase was 70/30 methanol/water mixture flowing at 0.9 mL/min.

The fungicide adsorbed amount, q [mg/g], was calculated by:

$$q = \frac{C_i - C_f}{m} \quad (1)$$

where C_i [mg/L] and C_f [mg/L] are the initial and final fungicide concentrations in the supernatant, respectively, and m [g/L] is the clay/solution ratio used in the experiment.

Different mathematical models were employed to fit adsorption kinetics data: pseudo-first-order (PFO), pseudo-second-order (PSO), and intra-particle diffusion model (IPD) and Elovich equations (Appendix A in supplementary material).

The validity of the kinetic models was quantitatively checked by using a normalized standard deviation Δq (%) calculated by the following equation:

$$\Delta q[\%] = \sqrt{\frac{\sum\left[\left(q_t - q_{t,cal}\right)/q_t\right]^2}{n-1}} \times 100 \quad (2)$$

where q_t and $q_{t,cal}$ are the experimental and calculated fungicide adsorbed amounts, respectively, at each time t and n is the number of data points in the kinetic curve. The lower the Δq[%] value, the better the model fits (Saha et al. 2013).

The adsorption isotherms were performed using individual and binary fungicide solutions: contact time = 24 h; temperature = 25 °C, and different solid dosages (Table 1).

Particularly, individual adsorption isotherms (A) of both fungicides onto Mt-Cu and Mt were compared for a solid dosage of 1 g/L (Table 1). After centrifugation, the solid phases corresponding to the highest IMZ or TBZ initial concentrations studied (150 or 25 mg/L respectively) were rinsed with distilled water, air-dried, and stored for further analyses ("Sample characterization"). The pH of the suspensions

Table 1 Experimental conditions used over the adsorption kinetics and adsorption isotherm determinations

Type of experiment	Fungicide (adsorbate)	C_i [mg/L]	Clay (adsorbent)	Adsorbent m [g/L]	Contact time [min]	Name
Ads. kinetics (K)	TBZ	15	Mt-Cu	1	10–4320	K-Mt-Cu-1-TBZ
Ads. kinetics (K)	TBZ	20	Mt-Cu	0.1	10–4320	K-Mt-Cu-0.1-TBZ
Ads. kinetics (K)	IMZ	40	Mt-Cu	1	10–4320	K-Mt-Cu-1-IMZ
Ads. kinetics (K)	IMZ	100	Mt-Cu	0.1	10–4320	K-Mt-Cu-0.1-IMZ
Individual ads. isotherm (A)	TBZ	0.5–25	Mt	1	1440	A-Mt-1-TBZ
Individual ads. isotherm (A)	TBZ	0.5–25	Mt-Cu	1	1440	A-Mt-Cu-1-TBZ
Individual ads. isotherm (A)	TBZ	0.5–25	Mt-Cu	0.5	1440	A-Mt-Cu-0.5-TBZ
Individual ads. isotherm (A)	TBZ	0.5–25	Mt-Cu	0.1	1440	A-Mt-Cu-0.1-TBZ
Individual ads. isotherm (A)	IMZ	2.5–150	Mt	1	1440	A-Mt-1-IMZ
Individual ads. isotherm (A)	IMZ	2.5–150	Mt-Cu	1	1440	A-Mt-Cu-1-IMZ
Individual ads. isotherm (A)	IMZ	2.5–150	Mt-Cu	0.5	1440	A-Mt-Cu-0.5-IMZ
Individual ads. isotherm (A)	IMZ	2.5–150	Mt-Cu	0.1	1440	A-Mt-Cu-0.1-IMZ
Concurrent ads. isotherms (C)	TBZ	3–18 (0.015–0.089 mmol/L)	Mt-Cu	0.1	1440	C-Mt-Cu-0.1-TBZ
Concurrent ads. isotherms (C)	IMZ	4.5–26.5 (0.015–0.089 mmol/L)	Mt-Cu	0.1	1440	C-Mt-Cu-0.1-IMZ
Successive ads. isotherm (S)	TBZ	0.5–25	Mt-Cu-IMZ	0.1	1440	S-IMZ-TBZ
Successive ads. isotherm (S)	IMZ	2.5–150	Mt-Cu-TBZ	0.1	1440	S-TBZ-IMZ

measured before and after the adsorption experiment remained constant at 6.1 and 5.6 for IMZ and TBZ adsorptions on Mt-Cu, respectively, while pH changed from 6.8 to 8.5 and from 6.5 to 7.5 for IMZ and TBZ adsorption isotherms in Mt, respectively (Gamba et al. 2015, 2017a).

To study the effect of the adsorbent dose on TBZ and IMZ individual adsorption isotherms, the removal efficiency (E, %) (Eq. 3) was calculated for the highest fungicide concentration used (25 and 150 mg/L, respectively):

$$E\ (\%) = \frac{C_i - C_f}{C_i} \times 100\% \quad (3)$$

where C_i and C_f are the initial and final fungicide concentrations in the solution phase, respectively.

In successive adsorption isotherms (S), Mt-Cu-TBZ sample was used as adsorbent of IMZ, while Mt-Cu-IMZ was used as adsorbent for TBZ (Table 1). Also, the simultaneous and concurrent adsorption isotherms (C) on Mt-Cu sample of both fungicides at the same molar concentration were determined to evidence mutual synergic or antagonistic effects.

With the aim of comparing adsorbent-adsorbate affinities and the adsorbent performance, the experimental isotherm data were fitted to Langmuir and Freundlich mathematical models (Appendix A in supplementary material). Based on Langmuir model, it is possible to determine R_L parameter:

$$R_L = \frac{1}{1 + C_0 * k} \quad (4)$$

where k [L/mg] is the Langmuir constant and C_o is the highest initial fungicide concentration [mg/L]. R_L values between 0 and 1 are assigned to favorable adsorption process; R_L values higher than 1 indicate unfavorable adsorption process; $R_L = 1$ designates linear adsorption while $R_L = 0$ points out irreversible adsorption (Darvishi Cheshmeh Soltani et al. 2011).

Sample characterization

Adsorbents and adsorbed products (see Table 1) were characterized using several techniques.

Cu^{2+} contents before and after adsorption experiments were determined by digesting 1 g of solids in 20 mL of concentrated HNO_3 at 60 °C until evaporation. This procedure was repeated twice. The obtained solids were suspended in a diluted HNO_3:H_2O solution (1:1). The suspension was filtered and the supernatant recovered. The Cu^{2+} concentration in the

supernatant was determined by atomic absorption spectroscopy using SensAA dual GBC Sci. equipment.

XRD patterns (001 peak) were collected on random powder samples from 2 to 30° (2θ) with a counting time of 10 s/step and 0.02° (2θ) step size, using a Philips PW 1710 diffractometer, operated at 40 kV and 30 mA with CuK_α radiation ($\lambda = 0.154$ nm).

EPR measurements were performed at X-band on a Bruker EMX Plus Spectrometer at 20 °C. The spectrometer settings were as follows: microwave frequency 9.87 GHz, modulation field 100 kHz, modulation amplitude 4 G, microwave power 0.2 mW, and 2040 points of resolution. The number of scans in all the experiments was 100.

Single-crystal X-Ray diffraction data of IMZ-Cu^{2+} complex were collected at 100 K (− 173.2 °C), using a Bruker D8 Quest ECO diffractometer, Photon 50 detector with graphite-monochromated MoKα ($\lambda = 0.71073$ Å) radiation. Data collection strategy and data reduction followed standard procedures implemented in the APEX3 suite of programs. Fifteen thousand seven hundred fifty-one collected reflections and 5235 independent reflections were obtained, 3270 with $I > 2\sigma(I)$, R_{int} 0.08. Data were corrected empirically for absorption employing the multi-scan method implemented in APEX2 suite. The structure was solved using the program SHELXS-97 (Sheldrick 1990) and refined using the full-matrix LS procedure with SHELXL-2014/7 (Sheldrick 2007). Anisotropic displacement parameters were employed for non-hydrogen atoms. All H atoms were located at the stereo-chemically expected positions and they were refined using a riding model. LS weights of the form $w = 1/[\sigma^2(F_o^2) + (01191P)^2 + 12.0938P]$ where $P = (F_o^2 + 2F_c^2)/3$ were employed. $R\,[F^2 > 2\sigma(F^2)] = 0.08$, $wR(F^2) = 0.22$.

Results and discussion

Adsorption kinetics and adsorption isotherms

For the evaluation of kinetic models, the effect of reaction time on the adsorption of TBZ or IMZ was assessed within an elapsed time of 4320 min. When a solid dosage of 1 g/L (Table 1) was used, more than 99% of the fungicides were removed in the first 10 min (Fig. S1, Supplementary material section). Taking into account that the final concentrations in the supernatant were below the UV detection limit (0.0045 mg/L for TBZ and 0.117 mg/L for IMZ), it was decided to diminish the adsorbent dosage to 0.1 g/L and increase the fungicides C_i. The obtained data was shown in Fig. 2. PFO, PSO, Elovich, and IPD models were evaluated to fit experimental values. Each equation parameter, correlation coefficients (R^2), and standard deviation Δq (%) were listed in Table 2. PFO and IPD could not be fitted to the whole process; they were adjusted only to the first 270 and 60 min for IMZ and TBZ, respectively (Sen Gupta and Bhattacharyya 2011), and the parameters in Table 2 showed the results within that interval.

Figure 2 shows that increasing the reaction time to 270 min for IMZ and to 60 min for TBZ caused a rapid increase in the adsorption capacity, reaching adsorption capacities higher than 450 mg/g and 170 mg/g, respectively.

A way to evaluate the accuracy of PFO and PSO kinetics models is comparing the experimental adsorption capacities at equilibrium ($q_{e,exp}$) with those obtained from the fitting (q_e). PFO predicts lower values for the equilibrium adsorption capacity than those from the experimental data. Furthermore, the values of R^2 are far from 1, suggesting that the sorption process does not fit the first-order model.

The equilibrium adsorption capacities, q_e, obtained with PSO model are slightly more precise than those of PFO when comparing predicted results with experimental data. In addition, a decrease of Δq and R^2 values around 0.8 suggested that PSO is better than PFO to fit experimental data. The PSO model establishes that chemical sorption is the rate-controlling step (Fatimah and Huda 2013; Jing et al. 2013; Park et al. 2013; Wang et al. 2016; Sen Gupta and Bhattacharyya 2006; Cheung et al. 2001; Ng et al. 2003; Özacar and Şengil 2005; Pérez-Marín et al. 2007), suggesting that Cu^{2+}-fungicide complex formation would be the main adsorption process.

The Elovich equation is based on a general second-order reaction mechanism for heterogeneous adsorption processes. As could be seen from Table 2, this model provided the best fit to the experimental data ($R^2 > 0.9$ and Δq lower or similar than those obtained for PSO model). Elovich fitting to TBZ adsorption kinetic curve promoted higher α and lower β values than IMZ. Pérez-Marín et al. (2007) related α and β to the rate of chemisorption and the surface coverage, respectively. In that sense, a higher α value for TBZ would be assigned to faster chemisorption processes (reinforced by a higher k_2 value), while higher β values for IMZ would designate larger surface coverage, i.e., fewer adsorption sites available due to greater adsorption capacity.

Elovich implies that the active sites are heterogeneous in nature and therefore exhibit different activation energies for chemisorption (Cheung et al. 2001). Accordingly, the rate-controlling step of the adsorption process may be the coordination of nitrogen atoms in the fungicide structures with copper cations located in Mt permanent—interlayer—and variable—edges—charged sites..

Finally, the IPD equation did not provide a good fit to the experimental data (low R^2 and high Δq, Table 2). This fact indicated that intra-particle diffusion process does not control the adsorption process and, instead, is controlled by chemical reaction.

The adsorption isotherms of individual fungicides onto Mt-Cu at different adsorbent dosages were shown in Fig. 3. In

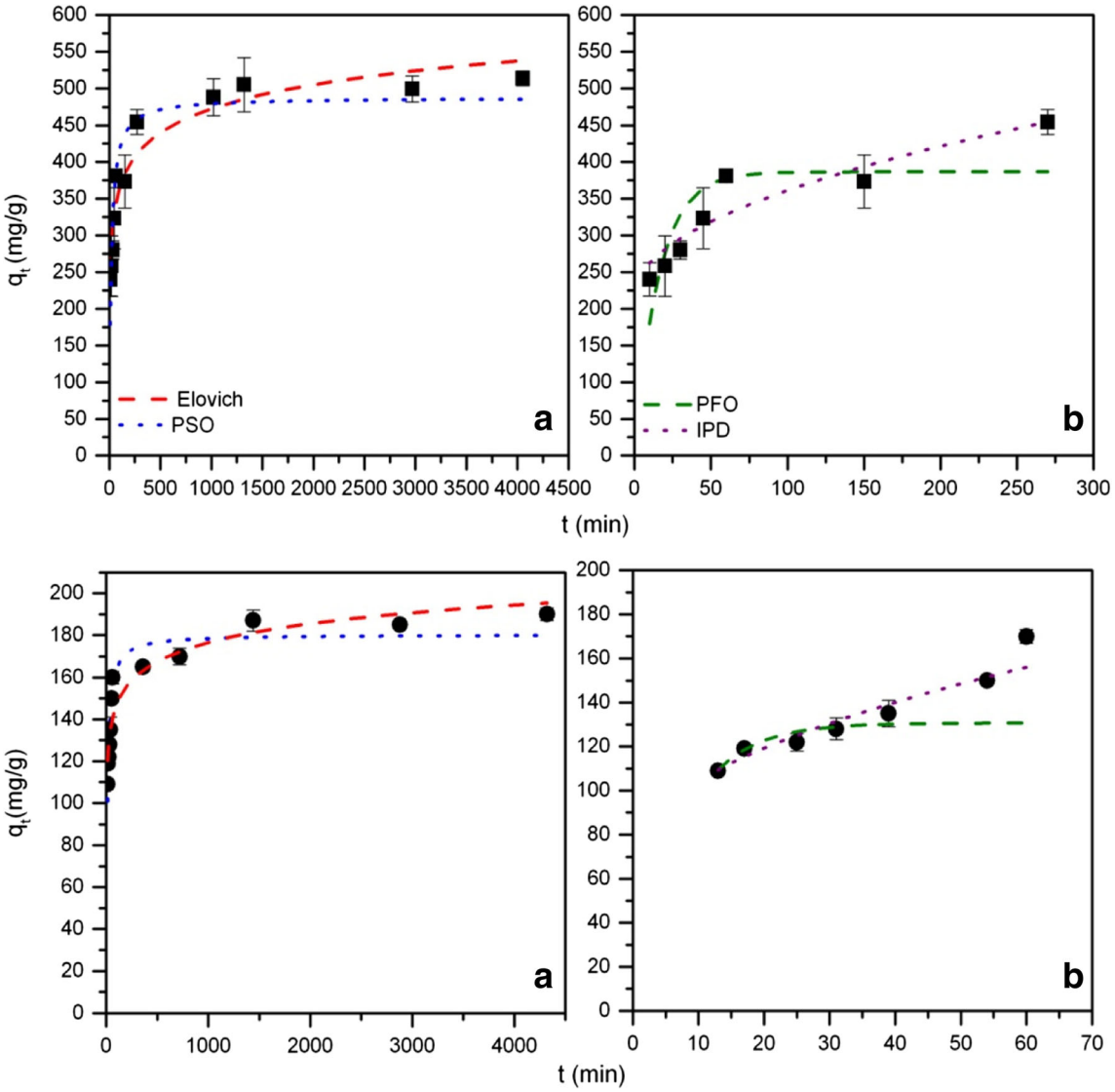

Fig. 2 Fungicide adsorption kinetics for Mt-Cu sample employing a solid dosage of 0.1 g/L. Symbols indicate as follows: (black square) IMZ and (black circle) TBZ. Lines correspond to (a) PSO and Elovich mathematical models fitted to the whole period of time; (b) PFO and IPD mathematical models fitted to the first minutes. Error bars represent standard deviations from triplicate experiments (error bars not evident are smaller than the symbols)

addition, their adsorption onto Mt employing a solid dosage of 1 g/L was added (Fig. 3a, d) with the aim of comparing the adsorbent performances at the highest solid dosage. R^2 and parameters obtained by Langmuir and Freundlich fittings for all adsorption systems, as well as the fungicide removal efficiencies (E, %), were listed in Tables 3, 4, and 5 for comparison.

Fungicide removal efficiencies (E) for C_i (TBZ) = 25 mg/L and C_i (IMZ) = 150 mg/L were higher than 90% when solid dosages equal to or greater than 0.5 g/L were used. These data are encouraging since it would be feasible to eliminate practically all the dissolved fungicide using Mt-Cu, if fungicide concentrations in water are lower than the concentrations evaluated in this work. Furthermore, the increase of E by almost 30% in Mt-Cu with respect to Mt (Table 3) demonstrated the role that the metal played in the removal of fungicides.

The Freundlich equation predicts that the fungicide concentrations on the adsorbent will increase as long as there is an increase in the fungicide concentration in the liquid. In this model, K_f and $1/n$ values can be used to show adsorption capacity and adsorption intensity, respectively (Ng et al. 2003). For the isotherms with solid dosage = 1 g/L, it was observed that both K_f and $1/n$ increased in Mt-Cu with respect to Mt for both fungicides, suggesting that both the capacity and the intensity of the fungicides in Mt-Cu is greater that for Mt. In addition, in all cases, $1/n$ values were less than 1, indicating non-linear behavior of adsorption.

For A-Mt-Cu-1-TBZ and A-Mt-Cu-0.5-TBZ isotherms, Langmuir fitting resulted in parameters with large associated

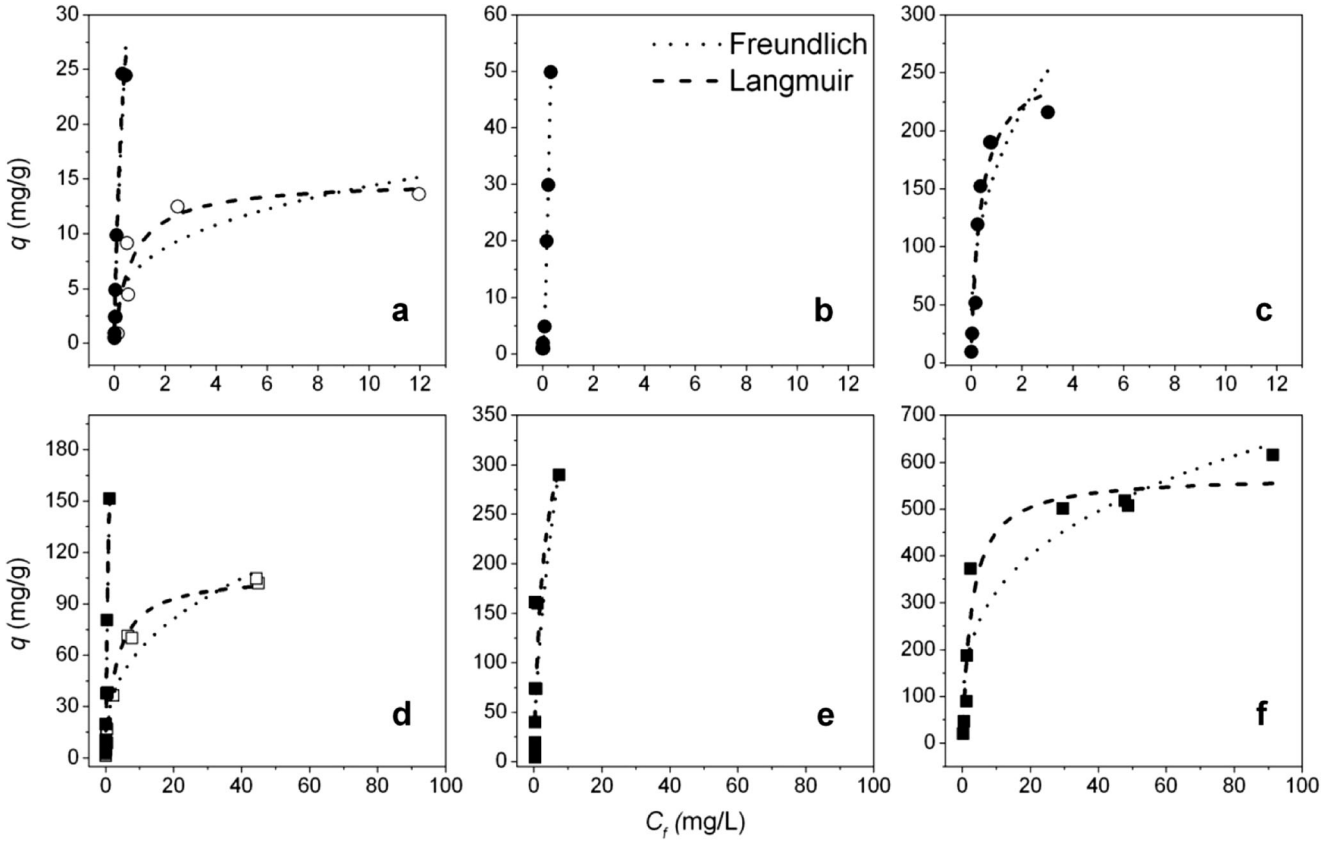

Fig. 3 Adsorption isotherms of TBZ onto (white circle) Mt and (black circle) Mt-Cu and IMZ onto (white square) Mt and (black square) Mt-Cu employing a solid dosage of **a**, **d** 1 g/L, **b**, **e** 0.5 g/L, and **c**, **f** 0.1 g/L. Lines correspond to Langmuir or Freundlich mathematical models fitted to experimental data

errors. It is necessary to remember that TBZ C_i (and therefore C_f) was limited by the solubility of the compound (25 mg/L). Langmuir isotherm model assumes a monolayer adsorption on a surface with a finite number of identical sites, where all sites

Table 2 Parameters, correlation coefficients (R^2), and standard deviation Δq (%) of mathematical models fitted to experimental data

Model	Parameter	TBZ	IMZ
	$q_{e,exp}$* [mg/g]	213 ± 7	536 ± 5
PFO	q_e [mg/g]	128 ± 5	$(39 \pm 3).10^1$
$q_t = q_e\left(1-e^{-k_1 t}\right)$	k_1 [1/min]	0.16 ± 0.05	0.06 ± 0.02
	R^2	0.073	0.356
	Δq [%]	35.78	19.78
PSO	q_e [mg/g]	$(180 \pm 1).10^1$	$(49 \pm 2).10^1$
$q_t = \frac{k_2 q_e^2 t}{1+k_2 q_e t}$	k_2 [g/-(mg min)]	$(6.5 \pm 0.2).10^{-4}$	$(1.2 \pm 0.3).10^{-4}$
	R^2	0.842	0.833
	Δq [%]	10.78	13.13
Elovich	α [mg/(-g min)]	$(10.0 \pm 0.5).10^2$	$(6 \pm 1).10^2$
$q_t = \frac{1}{\beta}\ln(\alpha\beta t)$	β [g/mg]	0.056 ± 0.008	0.021 ± 0.002
	R^2	0.953	0.918
	Δq [%]	12.22	8.53
IPD	k_{id} [mg/g min]	7 ± 1	14 ± 2
$q_t = k_{id} t^{0.5} + C$	C	$(8.0 \pm 0.5).10^1$	$(21 \pm 2).10^1$
	R^2	0.539	0.738
	Δq [%]	15.32	17.22

*It was determined by adsorption isotherms, using contact time = 24 h (1440 min) to ensure equilibrium

Table 3 Parameters and correlation coefficients of Freundlich and Langmuir models fitted to experimental TBZ and IMZ adsorption data and experimental fungicide removal efficiencies (E, %) for C_i (TBZ) = 25 mg/L, C_i (IMZ) = 150 mg/L, and adsorbent dosage = 1 g/L

Isotherm		A-Mt-1-TBZ	A-Mt-Cu-1-TBZ	A-Mt-1-IMZ	A-Mt-Cu-1-IMZ
Freundlich $q = K_f C_f^{1/n}$	K_f [L/mg]	7 ± 1	49 ± 6	27 ± 3	139 ± 9
	$1/n$	0.31 ± 0.09	0.8 ± 0.1	0.36 ± 0.03	0.7 ± 0.1
	R^2	0.747	0.956	0.920	0.962
Langmuir $q = \frac{q_{max} k C_f}{(1+kC_f)}$	q_{max} [mg/g]	15 ± 2	(5 ± 6).10^1	106 ± 6	(34 ± 9).10^1
	k [L/g]	1.5 ± 0.6	2 ± 1	0.33 ± 0.06	0.7 ± 0.3
	R_L	0.026	0.019	0.019	0.009
	R^2	0.879	0.977	0.955	0.974
E (%)		60.7 ± 0.3	98.7 ± 0.3	66.5 ± 0.2	99.3 ± 0.1

are energetically equivalent and without any interaction between adsorbed molecules. It also contemplates the formation of a *plateau* when the adsorption sites become saturated. In the isotherms abovementioned, no *plateau* was observed, possibly because C_f was not large enough to promote the adsorption site saturation. This fact could have originated the uncertainties in the parameters of the Langmuir model. Despite this fact, q_{max} increased at least twice, when a dosage of 1 g/L was used, in Mt-Cu isotherms in relation to Mt isotherms (Table 3). The Langmuir dissociation constant k was also higher for Cu-exchanged Mt than for raw Mt samples, indicating that the metal cation was involved in the fungicide adsorption process. This is in accordance with the hypothesis of coordination complex formation between Cu^{2+} and fungicide molecules.

The maximum fungicide adsorption capacities (q_{max}) were obtained with the minimum solid dosage (0.1 g/L). These results indicated that the accuracy of the Freundlich and Langmuir models fitting to the different systems depended on the experimental conditions (dosage of solid, fungicide, adsorbent). The values of q_{max} were higher than those published so far, both by our work group and others (Gamba et al. 2015, 2017b; Lombardi et al. 2003, 2006; Roca Jalil et al. 2013, 2014) suggesting that Mt-Cu has a significant potential for removal of fungicides from wastewater.

The increase of the solid dosage from 0.1 to 1 g/L promoted a decrease on q_{max} and an increase of E (Tables 3, 4, and 5) values. The increase of solid dosage supposed an increase of available adsorption sites for the fungicide uptake. However, many of these adsorption sites remained unsaturated and isotherm *plateaus* were not attained due to the limit imposed by the solubility of the fungicides. Furthermore, the increase of the adsorbent amount in a given volume may cause physical blockage of some adsorption sites. Although the number of adsorption sites per unit mass of adsorbent is independent of the adsorbent mass in the suspension, the number of available sites per unit mass of adsorbent mass could be reduced, as the effective surface area is likely to decrease. Therefore, the fungicide-adsorbed amount per unit mass of adsorbent diminished, explaining the fall of q_{max} parameter (Lombardi et al. 2003; Fruhstorfer et al. 1993; Kaya and Ören 2005; Akpomie and Dawodu 2014; Malamis and Katsou 2013).

In addition, from q_{max}, it could be stated that Mt-Cu adsorption capacity was higher for IMZ uptake than for TBZ uptake. However, the Langmuir dissociation constant, k, was higher for TBZ than for IMZ, indicating higher adsorption energy of the former than the last.

Finally, the R_L values calculated and presented in Table 3 indicate that the adsorption is favorable in all systems, and in

Table 4 Parameters and correlation coefficients of Freundlich and Langmuir models fitted to experimental TBZ and IMZ adsorption data and experimental fungicide removal efficiencies (E, %) for C_i (TBZ) = 25 mg/L, C_i (IMZ) = 150 mg/L, and adsorbent dosage = 0.5 g/L

Isotherm		A-Mt-Cu-0.5-TBZ	A-Mt-Cu-0.5-IMZ
Freundlich $q = K_f C_f^{1/n}$	K_f [L/mg]	(26 ± 2).10^1	(8 ± 2).10^1
	$1/n$	0.70 ± 0.07	0.6 ± 0.1
	R^2	0.996	0.678
Langmuir $q = \frac{q_{max} k C_f}{(1+kC_f)}$	q_{max} [mg/g]	(1 ± 3).10^2	(4 ± 1).10^2
	k [L/g]	0.3 ± 0.8	0.4 ± 0.2
	R_L	0.117	0.016
	R^2	0.931	0.717
E (%)		98.2 ± 0.1	92.5 ± 0.4

Table 5 Parameters and correlation coefficients of Freundlich and Langmuir models fitted to experimental TBZ and IMZ adsorption data and experimental fungicide removal efficiencies (E, %) for C_i (TBZ) = 25 mg/L, C_i (IMZ) = 150 mg/L, and adsorbent dosage = 0.1 g/L

Isotherm		A-Mt-Cu-0.1-TBZ	A-Mt-Cu-0.1-IMZ
Freundlich $q = K_f C_f^{1/n}$	K_f [L/mg]	$(17 \pm 2).10^1$	$(16 \pm 4).10^1$
	$1/n$	0.36 ± 0.09	0.31 ± 0.06
	R^2	0.758	0.874
Langmuir $q = \frac{q_{max} k\ C_f}{(1+kC_f)}$	q_{max} [mg/g]	$(26 \pm 3).10^1$	$(57 \pm 3).10^1$
	k [L/g]	2.7 ± 0.4	0.4 ± 0.1
	R_L	0.014	0.016
	R^2	0.931	0.936
E (%)		87.7 ± 0.2	37.2 ± 0.7

some cases where this value tends to zero, it would also be irreversible (Darvishi Cheshmeh Soltani et al. 2011).

In Fig. 4, individual (A), concurrent (C), and successive (S) adsorption isotherms next to their respective Langmuir and Freundlich fitting curves were presented, to compare the effect of the presence of the second compound in the suspension, previously or simultaneously adsorbed. The correlation coefficient R^2 and the Langmuir and Freundlich parameters were listed in Table 6. To compare the performances of the adsorbent towards IMZ and TBZ, the parameters K_f, k, and q_{max} were expressed in liters per millimole and millimoles per gram, respectively, since the fungicides have different MW.

The presence of a second compound (Fig. 4) led to a decrease of q in the C_f range studied, for both fungicides, compared to their individual adsorption isotherms. This behavior may discard synergic effects, and instead, competition for the same adsorption sites may be proposed (Fan et al. 2014). Nevertheless, individual and multiple adsorption isotherms for IMZ and TBZ showed different behaviors. On one hand, q values for IMZ isotherms decreased following the trend: A-Mt-Cu-0.1-IMZ > S-Mt-Cu-0.1-IMZ > C-Mt-Cu-0.1-IMZ (i.e., IMZ adsorbed amounts were higher in the individual adsorption isotherm, followed by the sequential adsorption isotherm, and at last the concurrent adsorption isotherm). On the other hand, q values for TBZ isotherms decreased following the trend: A-Mt-Cu-0.1-TBZ > C-Mt-Cu-0.1-TBZ > S-Mt-Cu-0.1-TBZ (i.e., TBZ adsorbed amounts were higher in the individual adsorption isotherm, followed by the concurrent adsorption isotherm, and at last the sequential adsorption isotherm; Fig. 4). In agreement with these observations, q_{max} and K_f parameters, which measure the adsorption capacity, also followed the abovementioned trends.

To rationalize these differences, it is important to take into account that the adsorbed fungicide/copper content ratio in the adsorbed samples was 1.84 for Mt-Cu-IMZ and 0.43 for Mt-Cu-TBZ (Table 7). If the metallic center is considered the actual adsorption sites, ideally all Cu^{2+} ions were occupied in Mt-Cu-IMZ, limiting the further TBZ adsorption due to a saturation of adsorption sites in sequential adsorption isotherm (S-IMZ-TBZ). In contrast, only 43% of the adsorption sites were occupied in the Mt-Cu-TBZ sample, being 57% of the metallic centers available for the further adsorption of IMZ (S-TBZ-IMZ isotherm). This phenomenon explained why q_{max} and K_f values were higher for IMZ than for TBZ in sequential adsorption isotherms.

It is worth noting that the removal of pre-adsorbed fungicides in the sequential isotherms was less than 1.5×10^{-3} mmol/g, suggesting the possibility of using the same

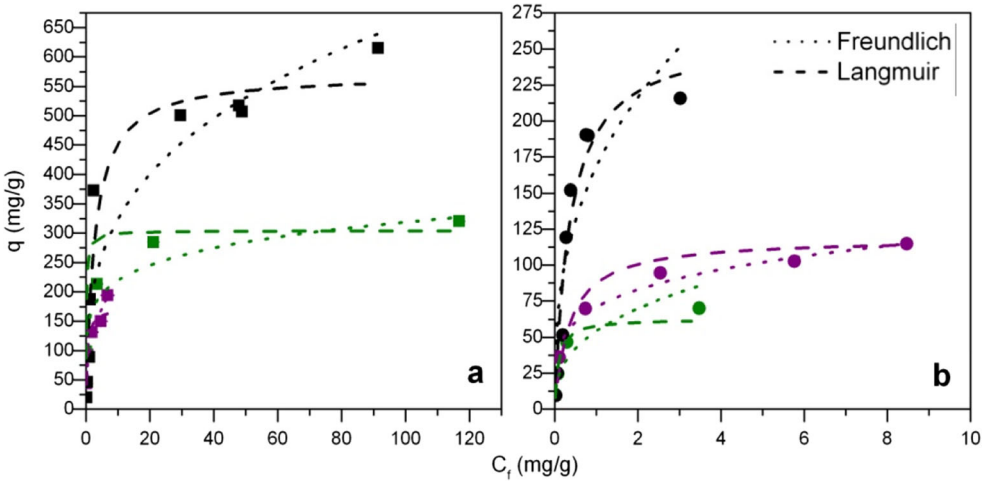

Fig. 4 Multiple adsorption isotherms of **a** IMZ: (■) A-Mt-Cu-0.1-IMZ, (■) S-TBZ-IMZ, and (■) C-Mt-Cu-0.1-IMZ and **b** TBZ: (●) A-Mt-Cu-0.1-TBZ, (●) S-IMZ-TBZ, and (●) C-Mt-Cu-0.1-TBZ. Lines correspond to Langmuir of Freundlich fits

Table 6 Parameters and correlation coefficients of Langmuir-Freundlich (LF) models fitted to multiple adsorption isotherms

	TBZ			IMZ		
Isotherm	A-Mt-Cu-0.1-TBZ	C-Mt-Cu-0.1-TBZ	S-IMZ-TBZ	A-Mt-Cu-0.1-IMZ	C-Mt-Cu-0.1-IMZ	S-TBZ-IMZ
Freundlich						
K_f [L/mmol]	0.85 ± 0.09	0.35 ± 0.01	0.27 ± 0.04	0.52 ± 0.01	0.033 ± 0.02	0.51 ± 0.02
$1/n$	0.36 ± 0.9	0.23 ± 0.02	0.36 ± 0.05	0.31 ± 0.06	0.35 ± 0.04	0.163 ± 0.009
R^2	0.758	0.985	0.844	0.874	0.942	0.985
Langmuir						
q_{max} [mmol/g]	1.3 ± 0.1	0.47 ± 0.01	0.31 ± 0.03	1.9 ± 0.1	0.67 ± 0.03	1.01 ± 0.07
k [L/mmol]	0.013 ± 0.003	0.015 ± 0.005	0.055 ± 0.009	$(1.3 \pm 0.3).10^{-3}$	0.008 ± 0.001	0.020 ± 0.003
R^2	0.931	0.912	0.956	0.936	0.964	0.944

material (Mt-Cu) in the sequential treatments of effluents containing different fungicides.

In concurrent adsorption isotherms, whereas the same initial concentration was used for both fungicides, q_{max} and K_f values were higher for C-Mt-Cu-0.1-IMZ isotherms than for C-Mt-Cu-0.1-TBZ (Table 6), showing that the material presented a higher adsorption capacity towards IMZ than TBZ. This phenomenon could be due to the monodentate behavior of IMZ and the bidentate behavior of TBZ. However, the dissociation constant k in the binary system was higher for TBZ than for IMZ (Table 6), indicating stronger adsorption energies for the former than for the last. Changes in k values in binary systems in comparison to those obtained for individual adsorption systems may be caused by the presence of a second fungicide in the suspension that alters the relative affinities between the material and the molecules.

Summarizing, the Cu^{2+} presence in Mt-Cu rose the TBZ and IMZ adsorption capacities compared to raw Mt, suggesting its participation in the fungicide uptake. Taking into account that pH remained constant during the adsorption experiment, it is evident that there were no acid-based reactions and probably the neutral form of the molecules was involved in the adsorbent/adsorbate interaction. It was evidenced from the multiple adsorption isotherms that there was a competition for the same adsorption sites between both fungicides (antagonistic effects). Additionally, the amount of adsorption sites available for IMZ in Mt-Cu was higher than that of the sites available for TBZ in the same adsorbent. This could be due to the bidentate ligand behavior of TBZ (Grevy et al. 2002), while the first would behave as a monodentate ligand (Holešová et al. 2009).

Sample characterization

Initial fungicide concentration and solid dosage used to obtain the characterized samples, as well as the final fungicide and/or copper contents in them, were resumed in Table 7.

It is evident that if the cation exchange reaction proposed for IMZ and TBZ uptake by Mt was valid also for Mt-Cu sample, the copper removal should have been the same amount as the adsorbed fungicide. But this phenomenon was not observed. More than 87% of the initial copper content was remained in the solid after fungicide adsorption. This reinforces the hypothesis that coordination between copper and the neutral form of the molecules is the mechanism that took place.

Changes in the interlayer of adsorbed samples were assessed by the shift of 001 peak in X-ray diffraction patterns, which were turned into basal spacing through Bragg equation (Table 7). The Cu^{2+} incorporation in the interlayer led to a basal spacing of 1.26 nm and was attributed to $[Cu(H_2O)_6]^{2+}$ complex (Brtáňová et al. 2014; Joseph-Ezra et al. 2014). In a previous work (Gamba et al. 2017b), it was reported that the adsorption of TBZ shifted the 001 peak to lower angles, evidencing its interlayer entrance. The widening of the peak

Table 7 Fungicide initial concentration (C_i) and adsorbed amount (q), copper content (Cu^{2+}), adsorbed fungicide/copper content ratio (q/Cu^{2+}), and basal space of characterized samples

Sample	C_i [mg/L]	q [mmol/g]	Cu^{2+} [mmol/g]	q/Cu^{2+}	Basal space (nm)
Mt	n.a.	n.a.	n.a.	n.a.	1.16
Mt-Cu	n.a.	n.a.	0.31 ± 0.02	n.a.	1.26
Mt-Cu-TBZ	25	0.121 ± 0.002	0.28 ± 0.04	0.43	1.47; 1.31
Mt-Cu-IMZ	150	0.498 ± 0.007	0.27 ± 0.03	1.84	1.47
Mt-TBZ	25	0.068 ± 0.003	n.a.	n.a.	1.51
Mt-IMZ	150	0.390 ± 0.005	n.a.	n.a.	1.50

n.a. not applicable

obtained for Mt-Cu-TBZ sample suggested the existence of two different 001 peaks. The first conducted to a basal space of 1.47 nm, similar to that obtained in TBZ intercalated Mt (1.51 nm) where a parallel orientation of the molecule between siloxane layers was assigned (Lombardi et al. 2003, 2006; Roca Jalil et al. 2013). This peak in Mt-Cu-TBZ sample was specifically attributed in Gamba et al. (2017b) to TBZ-Cu^{2+} complex which could be developed by a ligand exchange between water molecules from the hydration sphere of copper ions and TBZ. The decrease of water molecules in the interlayer explains the decrease of the interlayer space related to Mt-TBZ. The second peak led to a basal spacing of 1.31 nm, assigned to $[Cu(H_2O)_6]^{2+}$ complex that remained in the interlayer without reacting (Brtáňová et al. 2014; Joseph-Ezra et al. 2014). It is worth noting that the ratio TBZ/Cu^{2+} in Mt-Cu-TBZ sample was 0.43 (Table 7), indicating that even if each Cu^{2+} center was bonded to one TBZ molecule, there would remain 0.19 mmol/g of Cu^{2+} as $[Cu(H_2O)_6]^{2+}$ explaining the two 001 values obtained.

The IMZ adsorption in Mt-Cu sample led to a unique 001 reflection peak corresponding to a basal space of 1.47 nm, similar to the 1.50-nm value obtained for Mt-IMZ sample. In Mt-Cu-IMZ sample, the ratio IMZ/Cu^{2+} was 1.84 (Table 7), meaning that if all the IMZ molecules were in the interlayer space, the totality of the metallic centers would be bonded at least to one IMZ molecule (the most of them would be bonded to two IMZ molecules). This explained the fact that the 001 peak associated to $[Cu(H_2O)_6]^{2+}$ complex was absent in this sample.

In order to study the coordination sphere of the Cu^{2+} centers in the clay structure before and after the IMZ or TBZ uptake by the Mt-Cu material, X-band EPR spectra were performed and the results were shown in Fig. 5. The Cu^{2+} ions were adsorbed to different sites in the Mt structure. The signal at $g = 2.12$ was attributed to free hydrated Cu^{2+} ions or coordinated with hydroxyl groups and/or water molecules in the interlayer of the Mt structure (He et al. 2001; Heller-Kallai and Mosser 1995). The other signal at $g = 2.07$ was associated to the specific adsorption of Cu^{2+} to the hexagonal cavities of Mt according to previous results reported in He et al. (2001). When IMZ and TBZ were coordinated with the copper centers, similar EPR changes were observed due to the electronic density modifications in the surrounding of the metal ion. In fact, IMZ and TBZ displaced water molecules and/or hydroxyl groups responsible from being the anchor ligands of copper centers in the Mt structure. Hence, the EPR lines reflect that the coordination sphere of copper is changing due to the shift to high field values of the EPR lines associated to the nitrogen active role in the coordination to copper that increased the $A_{//}$ values and reduced the $g_{//}$ values in comparison with the oxygen surrounding of the paramagnetic center in the Cu-Mt sample before the addition of TBZ or IMZ (Gamba et al. 2017b; Heller-Kallai and Mosser 1995; Donoso et al. 2013). Although the high density of Cu^{2+} affected the resolution in the hyperfine region, an $A_{//}$ constant can be estimated in ~ 160 G for the Cu^{2+} centers in Mt-Cu-IMZ sample, which was similar to those reported in a rich nitrogen coordination sphere for some copper complexes in ethylenediamine-

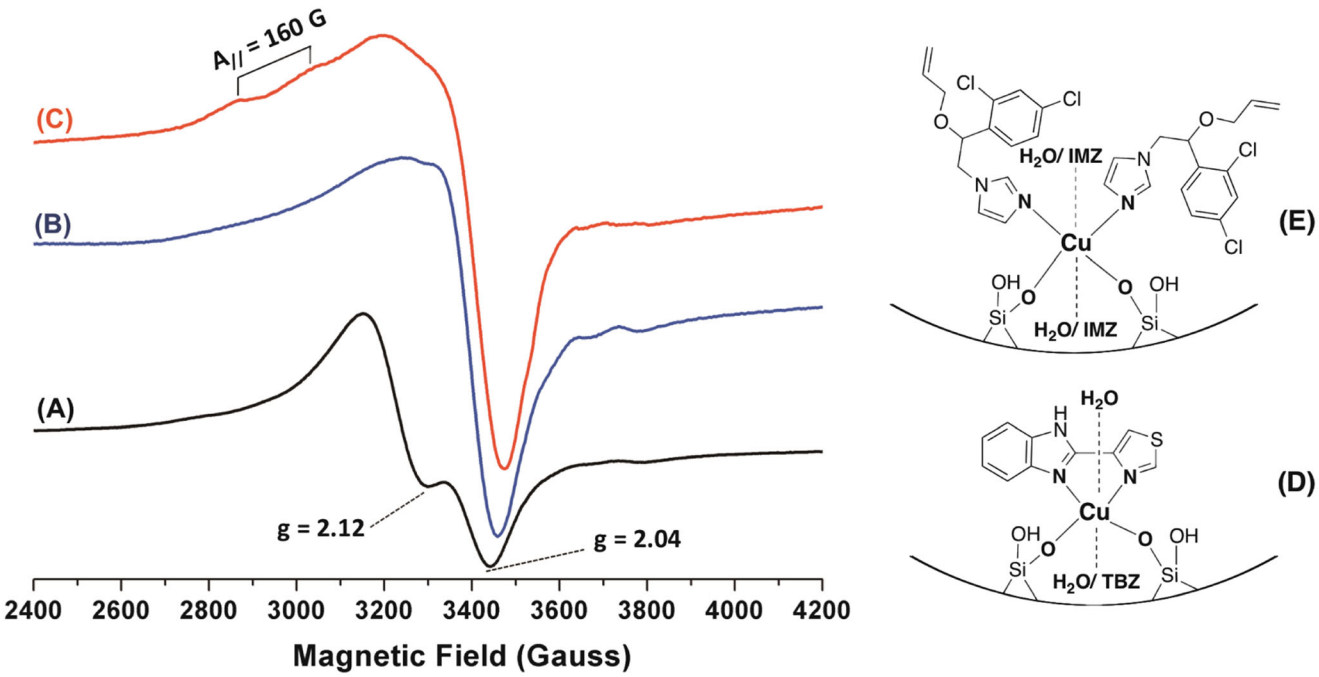

Fig. 5 EPR spectra for the Mt-Cu (A), Mt-Cu-TBZ (B), and Mt-Cu-IMZ (C) solid samples. Possible chemical structures for the copper centers in the Mt-Cu-TBZ (D) and Mt-Cu-IMZ (E)

bentonite (Donoso et al. 2013), imidazole-containing polymers (Lázaro-Martínez et al. 2013), and mesoporous silica (Abry et al. 2009). On the other hand, a broad and unresolved hyperfine EPR signal was observed due to the proximity of the paramagnetic Cu^{2+} centers suffering spin-orbit and exchange interactions in Mt-Cu-TBZ sample (Fig. 5).

Single-crystal X-ray diffraction studies

The single-crystal of IMZ-Cu^{2+} complex was obtained in order to access to the coordination modes and also as a model to predict the uptake of imazalil molecules by the copper ions supported in the Mt structure. The copper centers presented a square planar geometry where four IMZ molecules were bounded to the paramagnetic center through the pyridinic-type nitrogen of the imidazole moieties with nitrate ions present in the axial positions of the Cu sites (Fig. 6). The nitrate ions arose from the copper nitrate salt (Cu $(NO_3)_2$) used to obtain the single crystals. This fact makes a completely different panorama in comparison with TBZ-Cu^{2+} complexes reported in Wisniewski et al. (2001) where two molecules of TBZ were involved in the coordination of copper. This behavior may explain the higher uptake capacity of the Cu-Mt material for IMZ than for TBZ. Interestingly, the disposition of the IMZ molecules in the copper complex was not the same in the crystal structure due to the presence of the racemic mixture. The asymmetric unit contains two IMZ molecules with different configurations for the stereogenic centers C7A and C7B. The (*R*)-imazalil enantiomer presents an extended conformation, with N4-C6-C7-C8 torsion angle of 171.5°, showing the imidazole and benzene rings almost parallel and separated. Similar conformation was previously observed in the single-crystal structure for the free IMZ reported in Cheon et al. (2011). The (*S*)-imazalil enantiomer presents a closed conformation, with N4-C6-C7-C8 torsion angle of − 61.05°, inducing the approach of benzene to the imidazole ring (Fig. 6, Figs. S3 and S4).

Conclusions

In this study, a Cu^{2+}-exchanged montmorillonite was obtained through a simple and efficient process. The metal cation was bonded by electrostatic forces as free hydrated Cu^{2+} ions or coordinated with hydroxyl groups and/or water molecules in both inner and external Mt surfaces. The Mt-Cu material considerably improved TBZ and/or IMZ adsorption from aqueous suspensions with respect to raw Mt, leading to removal efficiencies higher than 99% after 10 min of contact time for TBZ and IMZ $C_i = 15$ and 40 mg/L, respectively, when a solid dosage = 1 g/L was used. These performances allowed decreasing the solid dosage, which could impact in decreasing the amount of generated solids after adsorption. Adsorption kinetics were obtained using solid dosage = 0.1 g/L, and experimental data fitted to Elovich and pseudo-second-order kinetics models. Both equations considered bond formation as the rate limiting step. TBZ adsorption process was achieved faster compared to the IMZ adsorption process. Also, from a thermodynamic point of view, TBZ adsorption was favored with respect to the adsorption found for IMZ (higher affinity constants), although the material showed more adsorption sites for IMZ than those available for TBZ (higher maximum

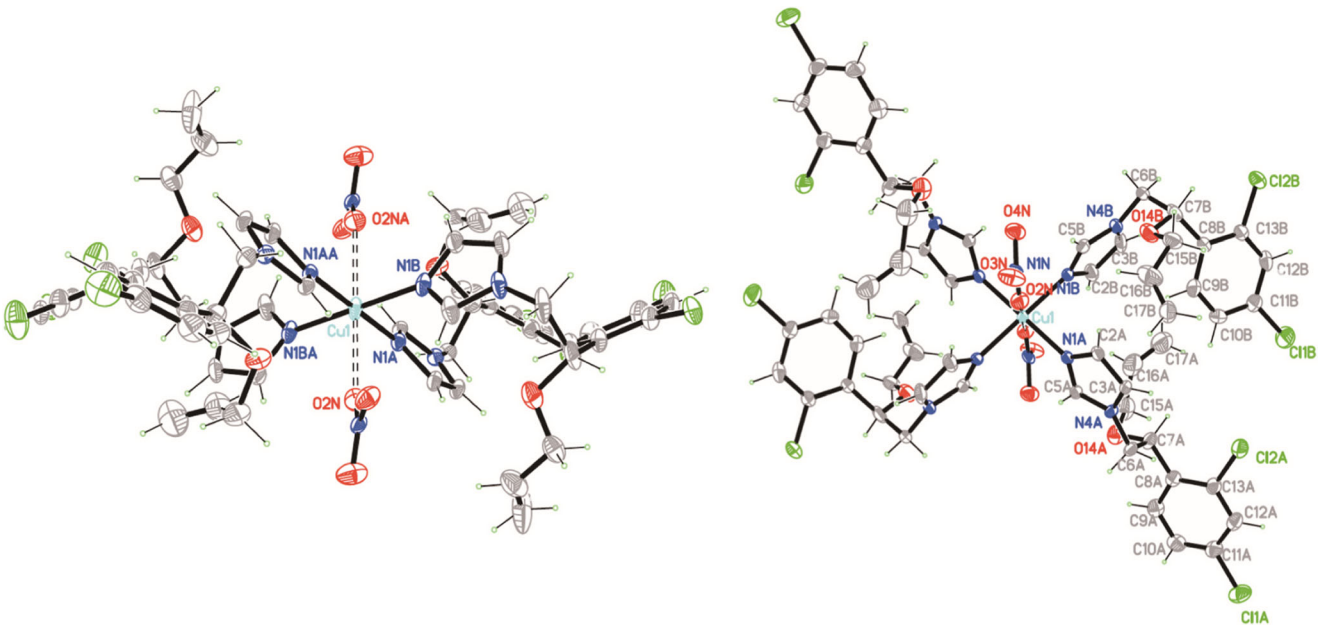

Fig. 6 Different visualizations of the crystal structure for the IMZ-Cu^{2+} complex. The displacement ellipsoids for the non-H atoms in the figure were drawn at the 50% probability level

amount adsorbed). Furthermore, Mt-Cu could remove both fungicides simultaneously and in a concurrent method from aqueous solution. It was evidenced that there were antagonistic effects when both fungicides were present in the solution, because they competed for the same adsorption sites.

From adsorption data and material characterization, it could be concluded that Cu^{2+} cations were the adsorption sites involved, while the rate limiting step was the formation of coordination bonds. The adsorption mechanism proposed is that of ligand exchange between water and fungicide molecules in the metal coordination sphere, as follows:

$$(\equiv X^-)_2\left[Cu(H_2O)_x\right]^{2+} + TBZ \leftrightarrow (\equiv X^-)_2\left[Cu(H_2O)_{x-2}(TBZ)\right] + 2H_2O \quad (5)$$

$$(\equiv X^-)_2\left[Cu(H_2O)_x\right]^{2+} + 2\ IMZ \leftrightarrow (\equiv X^-)_2\left[Cu(H_2O)_{x-2}(IMZ)_2\right] + 2H_2O \quad (6)$$

where $\equiv X^-$ are the permanent charged sites in the Mt internal surface.

The Mt-Cu developed in this study has a potential use in water treatment. Moreover, to obtain the adsorbent material, a sequential adsorption process might be considered: as first instance, the removal of heavy metals from mining/industrial effluents; as a second instance, the use of the adsorbed products for imidazolic and/or benzimidazolic derivative fungicide adsorption from agricultural effluents.

Acknowledgments The authors acknowledge the funding provided by FONARSEC project, Nano FS-008/2010, and ANPCYT (PICT 2016-1723), Univ. de Buenos Aires (UBACyT 2017-2019/22BA), and CONICET (PIP 2014-2016/130). GC, JLM, DV, and RMTS are members of CONICET, and MG, MO, and FY acknowledge the National Council of Scientific and Technical Research – CONICET, Argentina, for their respectively fellowships.

References

Abry S, Thibon A, Albela B, Delichère P, Banse F, Bonneviot L (2009) Design of grafted copper complex in mesoporous silica in defined coordination, hydrophobicity and confinement states. New J Chem 33:484

Akpomie KG, Dawodu FA (2014) Efficient abstraction of nickel (II) and manganese (II) ions from solution onto an alkaline-modified montmorillonite. J Taibah University Sci 8:343–356

Barahona F, Gjelstad A, Pedersen-Bjergaard S, Rasmussen KE (2010) Hollow fiber-liquid-phase microextraction of fungicides from orange juices. J Chromatography A 1217:1989–1994

Brtáňová A, Madejová J, Bizovská V, Komadel P (2014) Utilization of near infrared spectroscopy for studying solvation properties of Cu-montmorillonites. Spectrochim Acta A Mol Biomol Spectrosc 123: 385–391

Cheon S, Shin YW, Park KM, Kim J, Kim TH (2011) Imazalil: 1-[2-(2,4-Dichlorophenyl)-2-(Prop-2-Enyloxy)ethyl]-1 *H* –imidazole. Acta Crystallogr Sect E Struct Reports Online 67:1459–1459

Cheung CW, Porter LF, McKay G (2001) Sorption kinetic analysis for the removal of cadmium ions from effluents using bone char. Water Res 35:605–612

Darvishi Cheshmeh Soltani R, Rezaee A, Shams Khorramabadi G, Yaghmaeian K (2011) Optimization of lead (II) biosorption in an aqueous solution using chemically modified aerobic digested sludge. Water Sci Technol 63:129–135

de Oliveira Neto OF, Arenas AY, Fostier AH (2017) Sorption of thiabendazole in sub-tropical Brazilian soils. Environ Sci Pollut Res 24: 16503–16512. https://doi.org/10.1007/s11356-017-9226-8

Donoso P, Magon J, Lima JF, Rangel O, Benavente E, Moreno M, Gonzalez G (2013) Electron paramagnetic resonance study of copper-ethylenediamine complex ion intercalated in bentonite electron paramagnetic resonance study of copper-ethylenediamine complex ion intercalated in bentonite. J Phys Chem C 117:24042–24055

Environmental Protection Agency (EPA). https://www3.epa.gov/pesticides/chem_search/reg_actions/reregistration/fs_PC-111901_1-Feb-05.pdf

Environmental Protection Agency (EPA). https://www3.epa.gov/pesticides/chem_search/reg_actions/reregistration/fs_PC-060101_1-May-02.pdf

Fan H, Zhou L, Jiang X, Huang Q, Lang W (2014) Adsorption of Cu^{2+} and methylene blue on dodecyl sulfobetaine surfactant-modified montmorillonite. Appl Clay Sci 95:150–158

Fatimah I, Huda T (2013) Preparation of cetyltrimethylammonium intercalated Indonesian montmorillonite for adsorption of toluene. Appl Clay Sci 74:115–120

Fruhstorfer P, Schneider RJ, Weil L, Niessner R (1993) Factors influencing the adsorption of atrazine on montmorillonitic and kaolinitic clays. Sci Total Environ 138:317–328

Gamba M, Flores FM, Madejova J, Torres Sánchez RM (2015) Comparison of imazalil removal onto montmorillonite and nanomontmorillonite and adsorption surface sites involved: an approach for agricultural wastewater treatment. Ind Eng Chem Res 54: 1529–1538

Gamba M, Kovář P, Pospíšil M, Torres Sánchez RM (2017a) Insight into thiabendazole interaction with montmorillonite and organically modified montmorillonites. Appl Clay Sci 137:59–68

Gamba M, Olivelli M, Lázaro-Martínez JM, Gaddi G, Curutchet G, Torres Sánchez RM (2017b) Thiabendazole adsorption on montmorillonite, octadecyltrimethylammonium- and Acremonium sp.-loaded products and their copper complexes. Chem Eng J 320:11–21

Grevy JM, Tellez F, Bernés S, Nöth H, Contreras R, Barba-Behrens N (2002) Coordination compounds of thiabendazole with main group and transition metal ions. Inorg Chim Acta 339:532–542

Gürses A, Karaca S, Doğar Ç, Bayrak R, Açikyildiz M, Yalçin M (2004) Determination of adsorptive properties of clay/water system methylene blue sorption. J Colloid Interface Sci 269:310–314

He HP, Guo JG, Xie XD, Peng JL (2001) Location and migration of cations in Cu^{2+}-adsorbed montmorillonite. Environ Int 26:347–352

Heller-Kallai L, Mosser C (1995) Migration of Cu ions in Cu montmorillonite heated with and without alkali halides. Clay Clay Miner 43: 738–743

Holešová S, Kulhánková L, Martynková GS, Kukutschová J, Čapková P (2009) An effective route to montmorillonite intercalation with imidazole complexes: experiment and theory. J Mol Struct 923:85–89

Jiménez M, Ignacio Maldonado M, Rodríguez EM, Hernández-Ramírez A, Saggioro E, Carra I, Sanchez Perez JA (2015) Supported TiO2 solar photocatalysis at semi-pilot scale: degradation of pesticides found in citrus processing industry wastewater, reactivity and influence of photogenerated species. J Chem Technol Biotechnol 90: 149–157

Jiménez-Tototzintle M, Oller I, Hernández-Ramírez A, Malato S, Maldonado MI (2015) Remediation of agro-food industry effluents by biotreatment combined with supported TiO2/H2O2 solar photocatalysis. Chem Eng J 273:205–213. https://doi.org/10.1016/j.cej.2015.03.060

Jing P, Hou M, Zhao P, Tang X, Wan H (2013) Adsorption of 2-mercaptobenzothiazole from aqueous solution by organo-bentonite. J Environ Sci 25:1139–1144

Joseph-Ezra H, Nasser A, Mingelgrin U (2014) Surface interactions of pyrene and phenanthrene on Cu-montmorillonite. Appl Clay Sci 95: 348–356

Kaya A, Ören AH (2005) Adsorption of zinc from aqueous solutions to bentonite. J Hazard Mater 125:183–189

Lázaro-Martínez JM, Monti GA, Chattah AK (2013) Insights into the coordination sphere of copper ion in polymers containing carboxylic acid and azole groups. Polymer 54:5214–5221

Lombardi B, Baschini M, Torres Sánchez RM (2003) Optimization of parameters and adsorption mechanism of thiabendazole fungicide by a montmorillonite of North Patagonia, Argentina. Appl Clay Sci 24:43–50

Lombardi BM, Torres Sánchez RM, Eloy P, Genet M (2006) Interaction of thiabendazole and benzimidazole with montmorillonite. Appl Clay Sci 33:59–65

Magnoli AP, Tallone L, Rosa CA, Dalcero AM, Chiacchiera SM, Torres Sanchez RM (2008) Commercial bentonites as detoxifier of broiler feed contaminated with aflatoxin. Appl Clay Sci 40:63–71

Malamis S, Katsou E (2013) A review on zinc and nickel adsorption on natural and modified zeolite, bentonite and vermiculite: examination of process parameters, kinetics and isotherms. J Hazard Mater 252: 428–461

Mazloomi F, Jalali M (2017) Adsorption of ammonium from simulated wastewater by montmorillonite nanoclay and natural vermiculite: experimental study and simulation. Environ Monit Assess 189: 415. https://doi.org/10.1007/s10661-017-6080-6

Ng JCY, Cheung WH, McKay G (2003) Equilibrium studies for the sorption of lead from effluents using chitosan. Chemosphere 52: 1021–1030

Özacar M, Şengil İA (2005) A kinetic study of metal complex dye sorption onto pine sawdust. Process Biochem 40:565–572

Park Y, Ayoko GA, Kurdi R, Horváth E, Kristóf J, Frost RL (2013) Adsorption of phenolic compounds by organoclays: implications for the removal of organic pollutants from aqueous media. J Colloid Interface Sci 406:196–208

Parolo ME, Savini MC, Vallés JM, Baschini MT, Avena MJ (2008) Tetracycline adsorption on montmorillonite: pH and ionic strength effects. Appl Clay Sci 40:179–186

Pérez-Marín AB, Zapata VM, Ortuno JF, Aguilar M, Sáez J, Lloréns M (2007) Removal of cadmium from aqueous solutions by adsorption onto orange waste. J Hazard Mater 139:122–131

Roberts-Hutson C (ed) (1998) Metabolic pathways of agrochemicals. Insecticides and fungicides. The Royal Society of Chemistry, Cambridge

Roca Jalil ME, Vieira RS, Azevedo D, Baschini M, Sapag K (2013) Improvement in the adsorption of thiabendazole by using aluminum pillared clays. Appl Clay Sci 71:55–63

Roca Jalil ME, Baschini M, Rodríguez-Castellón E, Infantes-Molina A, Sapag K (2014) Effect of the Al/clay ratio on the thiabendazole removal by aluminum pillared clays. Appl Clay Sci 87:245–253

Rytwo G, Nir S, Margulies L (1995) Interactions of monovalent organic cations with montmorillonite: adsorption studies and model calculations. Soil Sci Soc Am J 59:554–564

Saha A, Tp AS, Gajbhiye VT, Gupta S, Kumar R (2013) Removal of mixed pesticides from aqueous solutions using organoclays: evaluation of equilibrium and kinetic model. Bull Environ Contam Toxicol 91:111–116

Sen Gupta S, Bhattacharyya KG (2006) Adsorption of Ni(II) on clays. J Colloid Interface Sci 295:21–32

Sen Gupta S, Bhattacharyya KG (2011) Kinetics of adsorption of metal ions on inorganic materials: a review. Adv Colloid Interf Sci 162: 39–58

Sheldrick GM (1990) Phase annealing in SHELX-90: direct methods for larger structures. Acta Crystallogr Sect A 46:467–473

Sheldrick GM (2007) A short history of SHELX. Acta Crystallogr Sect A Found Crystallogr 64:112–122

Tway PC, Love JC (1982) Effects of excited-state prototropic equilibria on the fluorescence energies of benzimidazole and thiabendazole homologues. J Phys Chem 86:5227–5230

Wang G, Su X, Hua Y, Ma S, Wang J, Xue X, Komarneni S (2016) Kinetics and thermodynamic analysis of the adsorption of hydroxy-Al cations by montmorillonite. Appl Clay Sci 129:79–87

Wisniewski MZ, Glowiak T, Opolski A, Wietrzyk J (2001) Synthesis, characterization and antiproliferative activity of the Co(II), Ni(II), Cu(II), Pd(II) and Pt(II) complexes of 2-(4-thiazolyl)benzimidazole (thiabendazole). Metal-Based Drugs 8:189–194